Journal of
Synchrotron Radiation

ISSN 0909-0495

Received 10 October 2011
Accepted 19 June 2012

A quantitative study of monochromatic X-ray transmission through zinc wires

Y. D. Wang,[a,b] A. W. Stevenson,[b] Y. S. Yang,[b]* A. Trinchi,[b] S. W. Wilkins,[b] Y. Q. Ren[a] and T. Q. Xiao[a]*

[a]Shanghai Institute of Applied Physics, Chinese Academy of Sciences, Shanghai 201800, People's Republic of China, and [b]CSIRO Materials Science and Engineering, Private Bag 33, Clayton South, Victoria 3169, Australia. E-mail: sam.yang@csiro.au, tqxiao@sinap.ac.cn

X-ray transmission through zinc wires of various diameters has been investigated systematically at different beam energies and sample-to-detector distances at the Shanghai Synchrotron Radiation Facility. This analysis shows that the experimentally measured transmission differs significantly from the theoretical estimation unless an appropriate point-spread function/line-spread function (PSF/LSF) is incorporated in the analysis. A number of other possible factors which may contribute to the observed inconsistencies were also assessed and these factors included higher harmonics and fluorescence; however, it was determined that these were not the dominant contributors underlying the inconsistencies. The investigation has demonstrated that the PSF/LSF is a major factor for consideration in quantitative X-ray micro-computed tomography.

Keywords: X-ray imaging; transmission; harmonic; fluorescence; PSF/LSF.

1. Introduction

Quantitative X-ray computed tomography (QCT) with synchrotron radiation is a powerful tool for non-destructive three-dimensional imaging, with various applications having been reported recently (Chen *et al.*, 2010; Qian *et al.*, 2005, 2008; Ohgaki *et al.*, 2007; Mayo *et al.*, 2010). Up to now, in-line X-ray phase-contrast imaging has been a popular imaging method for QCT, being widely adopted for research and applications in medical physics, biology, materials science and chemical dynamics, *etc.* (Wilkins *et al.*, 1996; Fitzgerald, 2000; Snigirev *et al.*, 1995; Tsai *et al.*, 2002; Gureyev *et al.*, 2001; Mayo *et al.*, 2002). Obtaining accurate X-ray transmission projection images is essential for faithful QCT reconstructions. Using a synchrotron-radiation-based monochromatic X-ray source and recording a large number of projection images over a series of view angles, it is possible to accurately reconstruct high-resolution three-dimensional maps of the absorption coefficient of a sample for a given X-ray beam energy. Such accurately reconstructed three-dimensional maps are paramount when attempting to resolve the three-dimensional microscopic distributions of different compositional phases in a materials sample. Image segmentation techniques, as well as other material phase prediction methods such as the data constrained modelling of a microstructure (Yang *et al.*, 2010*a*,*b*, 2011), rely heavily on the integrity of such data. However, owing to a number of experimental factors involved in the X-ray CT process, the accuracy of the measured X-ray transmission data can sometimes be compromised, thus leading to significant errors and inconsistencies in the absorption/attenuation coefficients of the reconstructed CT data.

In this communication we present our quantitative investigation on X-ray transmission through separate zinc wires of different diameters at a range of X-ray energies and sample-to-detector distances (SDDs). We observe significant differences between measured and theoretical X-ray transmission values, as obtained by simply applying equation (1). We then perform an analysis of the quantitative impact of a number of potential factors underlying the discrepancies including harmonic contamination, fluorescence and point-spread function/line-spread function (PSF/LSF).

2. Quantitative X-ray imaging experiments

The experiments were performed at beamline BL13W at the Shanghai Synchrotron Radiation Facility (SSRF; ring circumference 432 m, energy 3.5 GeV, current 200–300 mA). The sample stage was set at 34 m from the source (source-to-sample distance, R_1). High-purity zinc wires (99.9%, Goodfellow, K absorption edge at 9.659 keV) of various diameters (25, 50, 125 and 500 µm) were exposed to monochromatic X-ray beams of energies 9, 10, 10.5, 11, 11.5, 12, 15, 20, 25, 30 and 35 keV, at SDDs (R_2) of 2, 5, 10, 20, 50 and 100 cm. The flat-field and dark-current images were obtained at each energy and SDD for background correction. The white beam emanating from the wiggler source was monochromated using a double-crystal Si(111) monochromator with independent crystals. For different energies we also changed the wiggler gap. The combination of the CCD detector (with a native pixel size of 7.4 µm) with an optical lens (2×) provides an effective pixel size of 3.7 µm. The zinc wires were approximately vertically aligned, and the X-ray images were recorded by the detector, as shown in Fig. 1, from which the transmission information was obtained.

As the zinc wires are cylindrical, the transmission through the centre of a given wire corresponds to the absorption of zinc with the maximum thickness in the present experiments, *i.e.* the wire diameter (d). The minimum theoretical transmission (T) is simply estimated

Table 1
Comparisons of experimental and calculated transmissions for different energies and a SDD of 2 cm.

Zinc wire diameter (μm)	25 μm		50 μm		125 μm		500 μm	
Energy (keV)	Expt	Calc	Expt	Calc	Expt	Calc	Expt	Calc
9	0.57	0.44	0.35	0.20	0.14	0.02	0.08	9.0×10^{-8}
10	0.23	0.01	0.17	1.3×10^{-4}	0.11	2.0×10^{-10}	0.08	1.5×10^{-39}
10.5	0.23	0.02	0.17	3.4×10^{-4}	0.12	3.0×10^{-9}	0.09	8.3×10^{-35}
11	0.24	0.03	0.18	9.8×10^{-4}	0.12	3.0×10^{-8}	0.09	8.2×10^{-31}
11.5	0.26	0.05	0.17	2.1×10^{-3}	0.12	2.1×10^{-7}	0.08	2.0×10^{-27}
12	0.29	0.06	0.21	4.2×10^{-3}	0.14	1.1×10^{-6}	0.09	1.6×10^{-24}
15	0.40	0.22	0.21	0.05	0.13	5.7×10^{-4}	0.09	1.1×10^{-13}
20	0.69	0.51	0.48	0.26	0.22	0.03	0.10	1.4×10^{-6}
25	0.80	0.67	0.62	0.49	0.31	0.17	0.10	7.6×10^{-4}
30	0.86	0.81	0.72	0.65	0.46	0.34	0.10	0.01
35	0.90	0.87	0.81	0.76	0.56	0.50	0.18	0.06

from the total linear absorption coefficient (μ) (Brennan & Cowan, 1992; Zschornack, 2007) as

$$T = \exp(-\mu d) \quad (1)$$

in the absence of Fresnel diffraction.

Experimental and calculated transmission values at different energies for R_2 = 2 cm are shown in Table 1, and experimental and calculated transmissions at different SDDs for zinc wires with different diameters at an energy of 9 keV are shown in Table 2. It is evident from the tables that there are significant discrepancies between experimental transmission values and the corresponding calculated values. Such discrepancy becomes large when the total absorption is high. The results suggest that CT reconstructed linear absorption coefficients could be significantly lower than the expected values from standard data. Such an effect has been observed with some experimental samples studied with a laboratory-based X-ray source (Yang *et al.*, 2010*b*).

3. Analysis and numerical simulations

A number of factors could contribute to the discrepancies between theory and experiment, such as harmonic contamination, fluorescence and PSF. For a monochromatic X-ray beam from a double-crystal Si(111) monochromator, the second harmonic is very weak and the proportion of the third harmonic accounts for about 10% (Hart, 1980; Hou, 2005). For the 25 μm zinc wire, at an energy of 10 keV and a SDD of 2 cm, the calculated transmission is 0.09 when the third harmonic is considered. Moreover, this value could be lower when the two monochromator crystals are aligned independently and so harmonics can be suppressed. However, for the same conditions the experimentally measured transmission is 0.23. So the possibility that harmonics are the dominant factor underlying the discrepancy has been ruled out. When the material is irradiated by X-rays whose energy is higher than that of an absorption edge, it is possible to have

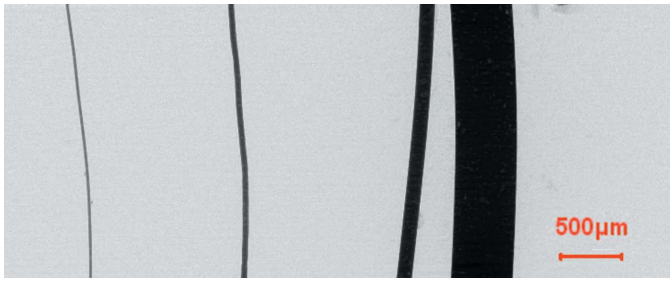

Figure 1
X-ray image of zinc wire samples at 9 keV and R_2 = 2 cm.

Table 2
Comparisons of experimental and calculated transmissions at different SDDs at an energy of 9 keV.

The last row provides the calculated values.

SDD (cm)	25 μm	50 μm	125 μm	500 μm
2	0.57	0.35	0.14	0.08
5	0.57	0.35	0.14	0.08
10	0.51	0.34	0.15	0.08
20	0.47	0.30	0.14	0.08
50	0.41	0.28	0.14	0.09
100	0.43	0.29	0.16	0.09
Calculated	0.44	0.20	0.02	9.0×10^{-8}

fluorescence emitted by the sample (Tertian, 1982). For the 25 μm zinc wire, at an energy of 10 keV and a SDD of 2 cm, the primary fluorescence component is calculated to be 0.049 and the fraction of the primary beam transmitted by the centre of the wire is 0.011, and so the apparent transmission is $(0.049 + 0.011)/(1 + 0.049) \simeq 0.058$. However, for the same conditions the experimentally measured transmission is 0.23. Furthermore, with increasing SDD, the fluorescence collected by the CCD should decrease quite markedly; however, this is not consistent with the experiment. Consequently fluorescence can be excluded as the primary cause of the observed discrepancies.

The next factor considered is the total PSF/LSF of the imaging system which arises due to the finite size of the source, the detector PSF and the geometrical magnification. Considering the X-ray beam to be totally incoherent, the measured intensity distribution at the CCD is the convolution of the 'ideal' image I_0 and the PSF, described as

$$I = I_0 * \mathrm{PSF}, \quad (2)$$

where PSF is the system's PSF referred to the image plane (Gureyev *et al.*, 2006; Peterzol *et al.*, 2007). As the zinc wire was approximately aligned vertically, the measured X-ray transmission is largely affected by the horizontal LSF. In order to investigate the effect of the PSF on the intensity distribution, the horizontal LSF of the imaging system was measured by the knife-edge method, with the SDD set to 2, 20 and 100 cm and the energy selected to be 9 and 20 keV (Zhu *et al.*, 1995).

The transmissions of zinc cylinders with diameters of 25, 50, 125 and 500 μm are calculated using equation (2) with corresponding experimental LSF. Comparison of experimental and simulated transmission function values, both with and without smearing by the PSF at 9 keV and SDD of R_2 = 2 cm, is shown in Fig. 2(*a*). It is found that the experimental transmission is very close to the simulated values with the effect of the PSF included, but differs significantly from the calculated values obtained without considering the PSF. On

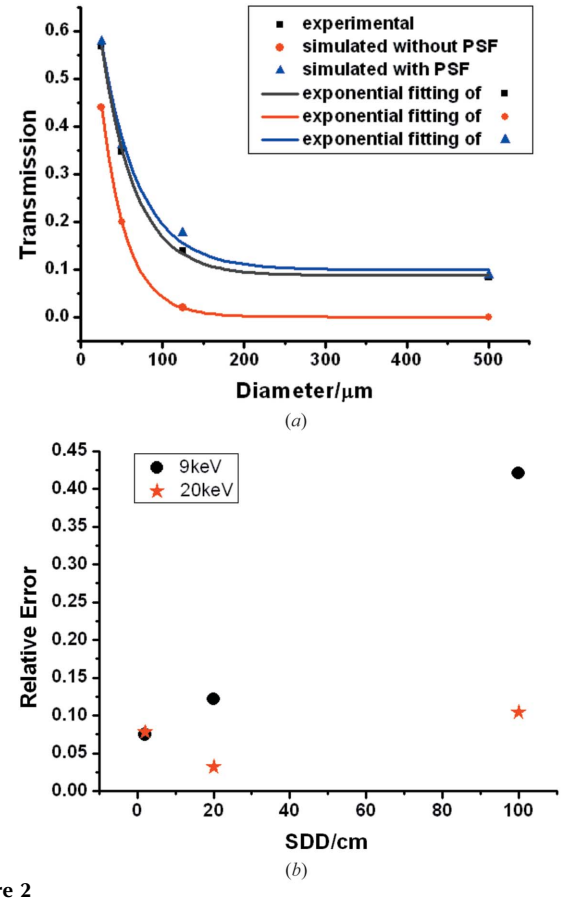

Figure 2
(*a*) Comparison of experimental and simulated transmission values at 9 keV and R_2 = 2 cm both without and with incorporation of the PSF. The lines are exponential fits of experimental transmission values (black), simulated transmission without (red) and with PSF (blue). (*b*) Graph of relative error between PSF-corrected and experimental values of the transmission as a function of SDD for the 9 keV and 20 keV cases.

this basis, the PSF/LSF is considered as the main factor accounting for the differences between the experimental and theoretical transmission values calculated according to equation (1).

The relative errors between experimental and simulated transmission with inclusion of the PSF are calculated and displayed in Fig. 2(*b*) for 9 keV and 20 keV, as a function of SDD. There is a trend that the relative error increases with increase of SDD, with the exception of the result for SDD = 20 cm and 20 keV. When the propagation distance is small, the diffraction effect is limited, and the system can be considered as totally incoherent. However, when the SDD is increased to 100 cm, the error is much larger than that obtained at an SDD of 2 cm because the system can no longer be considered to be totally incoherent, and the diffraction contribution is higher. It was also found that the relative error at 20 keV is smaller than that obtained at 9 keV, consistent with there being a smaller diffraction effect for higher X-ray energies, and so the system appears to be less coherent for the same SDD.

Source size and detector PSF can be estimated from the overall experimental PSF/LSF using simple geometrical arguments, and can be expressed as

$$\sigma_{\rm tot} = \left[\sigma_{\rm s}^2 (M-1)^2/M^2 + \sigma_{\rm d}^2/M^2\right]^{1/2}, \qquad (3)$$

where $\sigma_{\rm tot}^2$ is the variance of the experimental PSF/LSF and $M = (R_1 + R_2)/R_1$ is the geometric magnification (R_1 = 34 m). $\sigma_{\rm s}$ and $\sigma_{\rm d}$ refer to the source emissivity distribution ('source size') and detector PSF, respectively (Gureyev *et al.*, 2008; Stevenson *et al.*, 2010). For the PSF at each energy and SDD, we obtain the $\sigma_{\rm tot}$ value by fitting a Gaussian function. We use least-squares methods to refine the values of parameters $\sigma_{\rm s}$ and $\sigma_{\rm d}$ using these $\sigma_{\rm tot}$ values, the problem being overdetermined. The corresponding refined parameter values for the horizontal case are $\sigma_{\rm s(horiz)} = 198 \pm 15$ µm, $\sigma_{\rm d} = 3.5 \pm 0.4$ µm at 9 keV and $\sigma_{\rm s(horiz)} = 196 \pm 0.3$ µm, $\sigma_{\rm d} = 3.7 \pm 0.008$ µm at 20 keV, which means ${\rm FWHM}_{\rm s(horiz)} = 465 \pm 35$ µm, ${\rm FWHM}_{\rm d} = 8.2 \pm 0.94$ µm at 9 keV and ${\rm FWHM}_{\rm s(horiz)} = 460 \pm 0.7$ µm, ${\rm FWHM}_{\rm d} = 8.7 \pm 0.02$ µm at 20 keV. Calculations carried out at both energies yielded virtually identical values for the detector PSF, and the ${\rm FWHM}_{\rm d}$ over-determined value is approximately twice the actual detector pixel size (3.7 µm), which is reasonable. The estimated horizontal size of the source, calculated using *Shadow VUI* (Sanchez del Rio, 2001), is ${\rm FWHM}_{\rm s(horiz)} = 369$ µm at 9 keV and ${\rm FWHM}_{\rm s(horiz)} = 389$ µm at 20 keV, which is consistent with that of Zhao *et al.* (2005), and are somewhat smaller than the above experimental values.

4. Conclusion

A number of zinc wires with different diameters have been imaged at SSRF at various monochromatic X-ray beam energies and at different sample-to-detector distances. The analysis has shown that the transmission values measured in the experiment differ significantly from the theoretically calculated values unless appropriate PSFs/LSFs are incorporated in the analysis. Other conceivable contributing factors for the difference include harmonic contamination of the X-ray beam and fluorescence. However, the analysis indicates that they are not the dominant effects. The PSF is the key factor responsible for the differences between the experimental and theoretical transmission values, which is important for two-dimensional/three-dimensional quantitative imaging applications. In situations where PSF/LSF cannot be neglected, one should exercise caution in using X-ray CT-reconstructed data as a map of linear absorption coefficients.

The PSF of the imaging system is affected by source size, detector PSF and the geometrical magnification of the system. When the SDD is very small and the energy is high, the system can be treated as a totally incoherent system, so that the image at the detector plane is the convolution of PSF and geometrical transmission distribution. Furthermore, the source size and the PSF of the detector can be calculated from the system PSF. The values so obtained are quite reasonable and so provide a method to estimate source size and PSF of the detector. However, for the situations of lower energy and longer SDD, the system may no longer be treated as incoherent, with the result that some specialized algorithms should be used for extracting source and detector properties (see, for example, Gureyev *et al.*, 2008; Stevenson *et al.*, 2010).

Y. D. Wang would like to thank the Chinese Scholarship Council for sponsoring her visit to CSIRO during which this work has been carried out. She would also like to acknowledge the hospitality of CSIRO Division of Materials Science and Engineering. This work is partially sponsored by the CSIRO Computational and Simulation Science and Advanced Materials Transformational Capability Platforms.

References

Brennan, S. & Cowan, P. L. (1992). *Rev. Sci. Instrum.* **63**, 850–853.
Chen, R. C., Longo, R., Rigon, L., Zanconati, F., De Pellegrin, A., Arfelli, F., Dreossi, D., Menk, R. H., Vallazza, E., Xiao, T. Q. & Castelli, E. (2010). *Phys. Med. Biol.* **55**, 4993–5005.
Fitzgerald, R. (2000). *Phys. Today*, **53**, 23–26.

Gureyev, T. E., Mayo, S., Wilkins, S. W., Paganin, D. & Stevenson, A. W. (2001). *Phys. Rev. Lett.* **86**, 5827–5830.
Gureyev, T. E., Nesterets, Y. I., Paganin, D. M., Pogany, A. & Wilkins, S. W. (2006). *Opt. Commun.* **259**, 569–580.
Gureyev, T. E., Nesterets, Y. I., Stevenson, A. W., Miller, P. R., Pogany, A. & Wilkins, S. W. (2008). *Opt. Express*, **16**, 3223–3241.
Hart, M. (1980). *Lect. Notes Phys.* **112**, 325–335.
Hou, Z. C. (2005). *Rev. Sci. Instrum.* **76**, 013305.
Mayo, S. C., Miller, P. R., Wilkins, S. W., Davis, T. J., Gao, D., Gureyev, T. E., Paganin, D., Parry, D. J., Pogany, A. & Stevenson, A. W. (2002). *J. Microsc.* **207**, 79–96.
Mayo, S., Stevenson, A., Wilkins, S., Gao, D., Mookhoek, S., Meure, S., Hughes, T. & Mardel, J. (2010). *Proceedings of the 7th Pacific Rim International Conference on Advanced Materials and Processing*, Vol. 1–3, pp. 654–656, 2322–2325.
Ohgaki, T., Takami, Y., Toda, H., Kobayashi, T., Suzuki, Y., Uesugi, K., Makii, K., Takagi, T. & Aruga, Y. (2007). *Proceedings of the 6th Pacific Rim International Conference on Advanced Materials and Processing*, Vol. 1–3, pp. 561–565, 1677–1680.
Peterzol, A., Berthier, J., Duvauchelle, P., Ferrero, C. & Babot, D. (2007). *Nucl. Instrum. Methods Phys. Res. B*, **254**, 307–318.
Qian, L., Toda, H., Uesugi, K., Kobayashi, M. & Kobayashi, T. (2008). *Phys. Rev. Lett.* **100**, 115505.
Qian, L., Toda, H., Uesugi, K., Kobayashi, T., Ohgaki, T. & Kobayashi, M. (2005). *Appl. Phys. Lett.* **87**, 214208.
Sanchez del Rio, M. (2001). *Tutorials on XOP and SHADOWVUI*, http://ftp.esrf.eu/pub/scisoft/xop2.0/XopTutorial/exercises_xop+shadow.pdf.
Snigirev, A., Snigireva, I., Kohn, V., Kuznetsov, S. & Schelokov, I. (1995). *Rev. Sci. Instrum.* **66**, 5486–5492.
Stevenson, A. W., Mayo, S. C., Häusermann, D., Maksimenko, A., Garrett, R. F., Hall, C. J., Wilkins, S. W., Lewis, R. A. & Myers, D. E. (2010). *J. Synchrotron Rad.* **17**, 75–80.
Tertian, R. R. (1982). *Principles of Quantitative X-ray Fluorescence Analysis.* London: Heyden.
Tsai, W. L., Hsu, P. C., Hwu, Y., Chen, C. H., Chang, L. W., Je, J. H., Lin, H. M., Groso, A. & Margaritondo, G. (2002). *Nature (London)*, **417**, 139.
Wilkins, S. W., Gureyev, T. E., Gao, D., Pogany, A. & Stevenson, A. W. (1996). *Nature (London)*, **384**, 335–338.
Yang, S., Gao, D. C., Muster, T., Tulloh, A., Furman, S., Mayo, S. & Trinchi, A. (2010*b*). *Proceedings of the 7th Pacific Rim International Conference on Advanced Materials & Processing*, Vol. 1–3, pp. 654–656, 1686–1689.
Yang, Y. S., Gureyev, T. E., Tulloh, A., Clennell, M. B. & Pervukhina, M. (2010*a*). *Meas. Sci. Technol.* **21**, 047001.
Yang, Y. S., Liu, K. Y., Mayo, S., Tulloh, A., Clennell, B. & Xiao, T. Q. (2011). *J. Pet. Sci. Technol.* Submitted.
Zhao, Z. T., Xu, H. J. & Ding, H. (2005). *Proceedings of the 2005 Particle Accelerator Conference*, pp. 214–216.
Zhu, Y. M., Kaftandjian, V., Peix, G. & Babot, D. (1995). *Appl. Opt.* **34**, 4937–4943.
Zschornack, G. (2007). *Handbook of X-ray Data.* Berlin: Springer-Verlag.